Magnetoplasmon excitations in a two-dimensional square array of antidots

Danhong Huang
Department of Physics, The University of Lethbridge, Lethbridge, Alberta, Canada T1K 3M4

Godfrey Gumbs
Department of Physics and Astronomy, Hunter College and the Graduate Center, City University of New York, 695 Park Avenue, New York, New York 10021

(Received 14 July 1992)

The single-particle energy eigenvalues and eigenfunctions as well as the magnetoplasmon dispersion relation are calculated for a Landau quantized two-dimensional square array of antidots. Comparison is made with recent measurements of the magnetoplasmon excitation energies for antidots. Some unique features observed in the experiment of Kern *et al.* [Phys. Rev. Lett. **66**, 1618 (1991)] have been reproduced in numerical calculations and explained theoretically.

I. INTRODUCTION

Recently, submicrometer lithographic technology has been used to produce quantum dots which contain only a small number of electrons in discrete energy levels.[1-3] Various properties of quantum dots have been extensively studied, including the electronic eigenstates which have been obtained with the use of self-consistent calculations,[4] magnetoplasmon excitations,[5] magnetization instability,[6] magnetoresistance,[7] and many-particle tunneling.[8] The *reversed structure* to quantum dots is antidots which are obtained by etching an array of microscopic holes into a high-mobility two-dimensional (2D) electron-gas (EG) conductor.[9] The introduction of this strong spatially modulated potential leads to dramatic commensurability effects at low temperature in a uniform external magnetic field B.[10] In this array of artificial scatterers, there is pronounced structure in the magnetoresistance, anomalous low-field Hall plateaus, and a quenching of the Hall effect near $B=0$.[10] Kern *et al.*[9] have reported on the unique collective excitation spectrum of antidots. It consists of a high-frequency branch which starts with an oscillating and negative B dispersion and then increases in frequency with the magnetic field. A second low-frequency branch corresponds at high magnetic fields to edge magnetoplasmons which perform classical skipping orbits around the hole. There is anticrossing of the modes as the magnetic field increases. Some properties of antidots can be explained classically, but many interesting and anomalous features seem beyond the scope of simple electron orbit analysis. For example, the negative B dispersion and the oscillations near $B=0$ of the high-frequency mode[9] can only be explained quantum mechanically. With a simple model for antidots, we numerically calculate the single-particle energy eigenvalues and eigenfunctions for a square array of quantum antidots in the presence of a perpendicular magnetic field. We have found that there is a strong mixing of the Landau bands, due to the resonant coupling between umklapp scatterings. The peaks in the Fermi energy arise since some states in the Landau bands have been raised to higher energy levels. The calculated magnetoplasmon dispersion relation has qualitatively reproduced the negative B dispersion, as well as the oscillations and anticrossing observed in a recent experiment.[9]

The oscillating dispersion of the edge modes near $B=0$ is attributed to the oscillations in the single-particle Fermi energy and energy of the edge state, i.e., the resonant coupling between the umklapp scatterings. The negative dispersion of the edge modes near $B=0$ is a result of the removal of the degeneracy by the Coulomb interaction between the $2\omega_c$ cyclotron mode and the edge mode, which repel each other. It is also partly due to the increase of Landau-level degeneracy with magnetic field, which leads to the usual negative dispersion for edge modes. The anticrossing is directly attributed to the Coulomb interaction between the electrons, which is partially screened in the presence of weak scattering. The appearance of the $2\omega_c$ cyclotron mode is due to the fact that some degenerate states in the first two Landau levels have been raised to higher energy levels. The intensity of this optical transition is nonzero due to the mixing of the Landau wave functions.

The rest of this paper is organized as follows. In Sec. II, we describe our model for antidots and derive the eigenvalue equation for the single-particle energies of electrons in a quantizing external magnetic field. In Sec. III, we derive the dispersion relation for magnetoplasmons in a planar array of antidots. Section IV is devoted to the conclusions derived from the results of our calculations and some discussions.

II. SINGLE-PARTICLE EIGENSTATES

Our model consists of a 2D square array of quantum antidots with lattice constants a, in the x-y plane. The electrons with effective mass m^* are constrained to move in the x-y plane where the antidots, which we simulate by δ-function potential scatterers, are located. The magnetic field $\mathbf{B}$ is in the z direction, perpendicular to the plane containing the array. In the Landau gauge, the vector potential is given by $\mathbf{A}=Bx\hat{\mathbf{y}}$, where $\hat{\mathbf{y}}$ is a unit vector along the y axis and the Hamiltonian is

$$\mathcal{H}=\mathcal{H}_0+\mathcal{V}_{\rm Int}\ , \tag{1}$$

with free electron and interaction parts given, respectively, by

$$\mathcal{H}_0=\frac{1}{2m^*}(-i\hbar\nabla+eBx\hat{\mathbf{y}})^2 , \tag{2}$$

$$\mathcal{V}_{\rm Int}=V_0\sum_{j=-\infty}^{+\infty}\sum_{j'=-\infty}^{+\infty}\delta(x-ja)\delta(y-j'a) , \tag{3}$$

where the positive δ potential in the x-y plane simulates the 2D array of antidots. V_0/a^2 is the peak strength of these δ-function scatterers. The states for electrons with up and down spins are treated here as being degenerate, but spin effects can be incorporated into our formalism. For a homogeneous 2D EG in the absence of scatterers, the eigenstates are simply Landau wave functions, given by

$$\Psi^{(0)}(x,y)=\frac{e^{iky}}{\sqrt{2\pi}}\phi^{(0)}(x-X_0) , \tag{4}$$

with $\phi^{(0)}(x)$ satisfying the following equation:

$$\left[-\frac{\hbar^2}{2m^*}\frac{d^2}{dx^2}+\frac{m^*\omega_c^2}{2}(x-X_0)^2\right]\phi^{(0)}(x)=E^{(0)}\phi^{(0)}(x) , \tag{5}$$

where

$$\phi^{(0)}_{n,X_0}(x-X_0)=\left[\frac{1}{\pi^{1/2}2^n n!L_H}\right]^{1/2}\times\exp\left[-\frac{(x-X_0)^2}{2L_H^2}\right]H_n\left[\frac{x-X_0}{L_H}\right] , \tag{6}$$

$$E_n^{(0)}=(n+\tfrac{1}{2})\hbar\omega_c . \tag{7}$$

In this notation, k is the wave vector in the y direction, $\omega_c=eB/m^*$ is the cyclotron frequency, $L_H=(\hbar/eB)^{1/2}$ is the magnetic length, n is the Landau quantum number, and $X_0=-kL_H^2=-\hbar k/eB$ is the guiding center. In Eq. (6), $H_n(x)$ is the nth-order Hermite polynomial. When there are no scatterers, the energy eigenvalues are independent of the wave vector k. In our numerical calculations, we allow the continuous wave vector k to be discrete. Using periodic boundary conditions in the y direction, we have

$$k_m=\frac{2\pi}{a}\left[\frac{m}{N_y}\right] , \tag{8}$$

where $L_y=N_y a$ is the length of the 2D array in the y direction, and the quantum number $m=0,\pm1,\pm2,\ldots,\pm\infty$. We expand the eigenfunctions for the 2D array of antidots in terms of the complete set of Landau wave functions for a homogeneous 2D EG. This yields

$$\Psi(x,y)=\sum_{n,m}C_{n,m}\Psi^{(0)}_{n,m}(x,y) , \tag{9}$$

where the basis set is given by

$$\Psi^{(0)}_{n,m}(x,y)=\frac{\exp[i2\pi m(y/L_y)]}{\sqrt{L_y}}\phi^{(0)}_{n,m}(x-X_0^{(m)}) , \tag{10}$$

with $X_0^{(m)}=-2\pi a(L_H/a)^2(m/N_y)$. Furthermore, this basis set is orthonormal and the energy eigenvalues are the solutions of the secular equation

$$\mathcal{D}et\{(E_n^{(0)}-E)\delta_{n,n'}\delta_{m,m'}+\langle n',m'|\mathcal{V}_{\rm Int}|n,m\rangle\}=0 , \tag{11}$$

with

$$\langle n',m'|\mathcal{V}_{\rm Int}|n,m\rangle=\int_{-L_x/2}^{L_x/2}dx\int_{-L_y/2}^{L_y/2}dy\,\Psi^{(0)*}_{n',m'}(x,y)\mathcal{V}_{\rm Int}\Psi^{(0)}_{n,m}(x,y)$$
$$=\frac{V_0}{a}\delta(m-m'-lN_y)\sum_{j=-N_x/2}^{+N_x/2}\{\phi^{(0)}_{n',m'}(ja-X_0^{(m')})\phi^{(0)}_{n,m}(ja-X_0^{(m)})\} , \tag{12}$$

where $l=0,\pm1,\pm2,\ldots,\pm\infty$ stands for the contribution due to umklapp scattering. Here, we have assumed that the length of the 2D array in the x direction is $N_x a$. This imposes an upper limit on the quantum number m given by $|m|\le bN_xN_y/2$, where $b=\Phi/\phi_0$ is a scaled magnetic field with the flux quantum $\phi_0=h/e$ and $\Phi=Ba^2$ being the magnetic flux passing through the square region between antidots. The eigenfunctions can be obtained from the Jth eigenvector $\{C^J_{n,m}\}$, after numerically diagonalizing the matrix in Eq. (11). Since the eigenvector is normalized, we have $\sum_{n,m}|C^J_{n,m}|^2=1$ for any value of J. The scaled scattering strength is written as $u_0=2m^*V_0/(2\pi\hbar^2\sqrt{2})$. Also, we introduce the dimensionless variables $\bar{x}=x/a$, $\bar{y}=y/a$, and the scaled energy $\epsilon=E/\hbar\omega_c$. In a straightforward way, we obtain

$$\mathcal{D}et\{[(n+\tfrac{1}{2})-\epsilon]\delta_{n,n'}\delta_{m,m'}+\langle n',m'|v_{\rm Int}|n,m\rangle\}=0 , \tag{13}$$

where

$$\langle n',m'|v_{\rm Int}|n,m\rangle=\frac{\langle n',m'|\mathcal{V}_{\rm Int}|n,m\rangle}{\hbar\omega_c}$$

$$=\frac{u_0}{\sqrt{2^{n+n'}n!n'!b}}\delta(m-m'-lN_y)$$

$$\times\sum_{j=-N_x/2}^{+N_x/2}\left\{\exp\left[-\frac{\pi(jb+m/N_y)^2}{b}\right]\exp\left[-\frac{\pi(jb+m'/N_y)^2}{b}\right]\right.$$

$$\left.\times H_n\left[\frac{\sqrt{2\pi}(jb+m/N_y)}{\sqrt{b}}\right]H_{n'}\left[\frac{\sqrt{2\pi}(jb+m'/N_y)}{\sqrt{b}}\right]\right\}, \tag{14}$$

and the corresponding eigenfunction is

$$\Psi_J(\bar{x},\bar{y})=\frac{1}{a}\sum_{n,m}C^J_{n,m}\left[\frac{\sqrt{2b}}{2^n n!}\right]^{1/2}\exp\left[-\frac{\pi(\bar{x}b+m/N_y)^2}{b}\right]H_n\left[\frac{\sqrt{2\pi}[\bar{x}b+m/N_y]}{\sqrt{b}}\right]\frac{\exp[i2\pi(m/N_y)\bar{y}]}{\sqrt{N_y}}\ . \tag{15}$$

In our finite-size calculations, we truncate the set of quantum numbers $\{n,m\}$ by taking $|m|\le M_u$ and $n\le N_u$, where $M_u=bN_xN_y/2$. In this way, we have totally included bN_x Brillouin zones and the dimension of the matrix is $N_d=bN_xN_y(N_u+1)$. From these parameters, we can calculate the Fermi energy $E_F=E_{J=N_{\rm tot}/2}$, where $N_{\rm tot}=N_xN_ya^2n_{\rm 2D}$ is the total number of electrons in the square array and $n_{\rm 2D}$ is the areal electron density. In this notation, the charge-density distribution can be expressed as

$$\rho(\bar{x},\bar{y})=\sum_{1\le J\le N_{\rm tot}/2}|\Psi_J(\bar{x},\bar{y})|^2\ . \tag{16}$$

In our numerical calculations, we have taken

$$N_x=N_y=10\ ,\quad N_u=3\ ,\quad -5\le x\le 5\ ,\quad \text{and}\quad -5\le y\le 5\ .$$

When boundaries are introduced in the y direction, the wave vector k is discrete [see Eq. (8)]. The number of guiding centers between adjacent antidots varies from five to twenty over the range of magnetic fields used in our calculations. The results obtained only change by a few percent when N_y increases, for fixed values of N_x and N_u. The introduction of boundaries in the x direction is equivalent to putting two infinite potential barriers at $x=\pm N_xa/2$. When the amplitude of the wave function is large near the boundaries, we find the wave function changed with N_x. However, if the wave function only has a significant amplitude away from the boundary region, it is insensitive to the boundary change. Since there are many electrons in this array, the quantum number J for the topmost occupied state is large. We find that the amplitudes of the wave functions with large values of J are vanishingly small near the boundaries but large away from them. Throughout this paper, we are dealing with the low-lying excitations. Therefore, the topmost occupied state is taken to be the initial state for the excitations; the excitation energies as well as the form factors become insensitive to the value of N_x we are using. In choosing $N_u=3$ we are including four Landau levels. Here, we are concentrating on the transitions between the two lowest Landau bands. Only neighboring Landau levels are found to have significant mixing. As a result, the inclusion of four Landau levels is a good approximation. The convergence of the numerical results is ensured by requiring the final results to be insensitive to the choice of the parameters N_x, N_y, and N_u.

Figures 1(a) and 1(b) show the square of the eigenfunctions for different scattering strengths. The stronger the scattering, the more localized the eigenfunctions are in

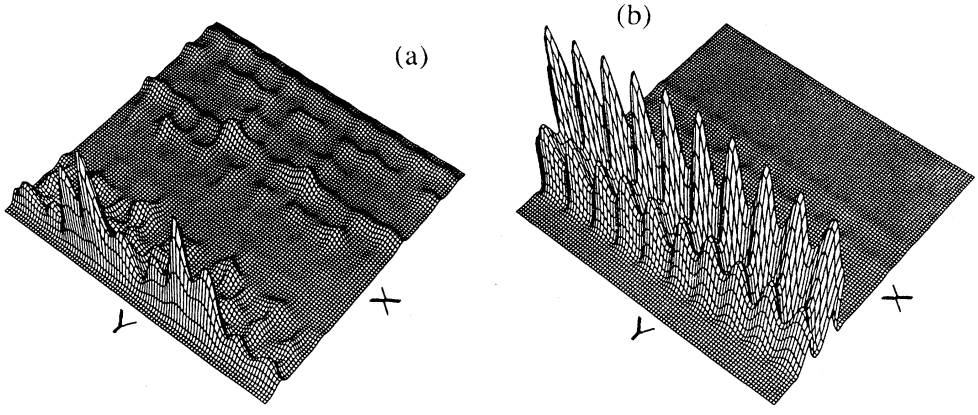

FIG. 1. The square of the eigenfunctions for different eigenstates, scattering strengths, and magnetic fields. Here, we have taken $N_x=N_y-10$, $N_u=3$, $-5\le x\le 5$, and $-5\le y\le 5$ in the calculations. Here, $J=10$ and $b=1.0$. (a) $u_0=2\times10^5$; (b) $u_0=1\times10^5$.

the y direction. For the ground state with $J=1$ in a weak magnetic field, the distributions of the eigenfunctions in the x and y directions are exponential and standing-wave-like, respectively. As the magnetic field b increases, this state gradually develops with its eigenfunction mainly distributed near the left-hand side of the 2D array. However, the spread in the x direction of the eigenfunctions for the excited states with $J \gg 1$ is large, but their evolution to an edge distribution is suppressed. The plane waves in the y direction, associated with various guiding centers in the Landau wave functions, experience correlated multiple reflections from the scatterers to form these scattering states. Under strong scattering and an intense magnetic field, we find a puddlelike distribution. For weak scattering, increasing the magnetic field can delocalize the eigenfunction in the x direction.

In Figs. 2(a) and 2(b), we plot the energy eigenvalue spectrum as a function of the reduced magnetic field b for different scattering strengths u_0. These results show that the original degenerate Landau levels are split and expanded into bands due to the removal of the degeneracy by scattering. The periodicity of the lattice potential in the y direction produces a gap at the Brillouin-zone boundary from the Bragg reflection. (This gap is not due to the discrete values of the wave vector k in the y direction, used in the numerical calculations.) The single-particle excitations discussed in this paper are related to the transitions between the two bands separated by this gap. There is strong mixing from the first two Landau bands in the presence of scatterers. When the scattering is strong, there exist eigenstates with negative energy at some specific value of magnetic field. This is due to the resonant coupling between umklapp scatterings in the Landau levels. As a duality of these negative-energy states, there also exist eigenstates with much higher energy. For weak scattering, an increase of magnetic field suppresses the mixing between the Landau bands. There are no eigenstates with negative energy in the weak-scattering case. When the guiding center is close to the scatterers, the related states will have much higher energy. Increasing u_0 produces the mixing. Although a strong magnetic field reduces the overlap of the Landau eigenfunctions at different scattering sites, it also increases the number of Brillouin zones participating in the umklapp scattering. Due to the resonant correlated multiple reflections, part of the degenerate states in the Landau levels is raised to the higher energy states.

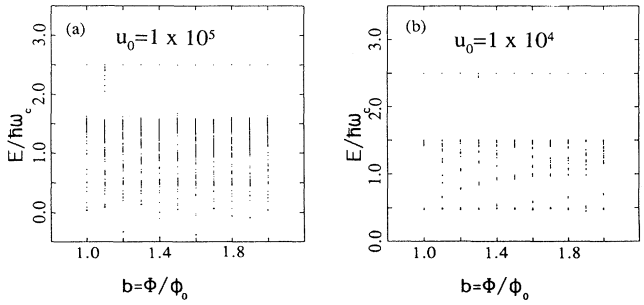

FIG. 2. The spectra of eigenenergies as a function of magnetic field for different scattering strengths. Here, we have used $N_x=N_y=10$, $N_u=3$, and $1\le b\le 2$ in the calculations. We have not shown the higher-energy levels, corresponding to the backward-scattering edge states. (a) $u_0=2\times10^5$; (b) $u_0=1\times10^4$.

In Fig. 3 we have plotted the Fermi energy as a function of magnetic field b for different scattering strengths u_0 and electron densities n_{2D}. The scatterers change a straight line into a decreasing and oscillating curve. The peak in this curve implies that some states in the Landau levels have been raised to higher energy levels. The peak is larger for the case with lower electron density.

Figures 4(a)–4(d) present the charge-density distributions for various values of scattering strengths, magnetic fields, and electron densities. Large magnetic fields greatly delocalize the charge-density distribution in the x direction under weak scattering, as shown in Fig. 4(a). Moreover, the edge distribution of the charge density is favored for strong magnetic fields. The higher electron density increases the spreading of the charge-density distribution near the central region along the x direction [see Figs. 4(b) and 4(c)], while the strong scattering sharpens this distribution in the same region [see Figs. 4(b) and 4(d)]. The charge-density distribution is almost uniform in the y direction compared to the x direction.

III. MAGNETOPLASMON EXCITATION ENERGIES

The results of our calculations for the single-particle energy eigenstates for an array of finite size are used to calculate the magnetoplasmon excitation energies for antidots for which the electron-electron interaction must be included. Assuming an external perturbation of the form

$$V^{\rm ext}(x,y,t)=\sum_{q_x,q_y} e^{i[\omega t-(q_x x+q_y y)]}V^{\rm ext}(q_x,q_y,\omega)\ , \qquad (17)$$

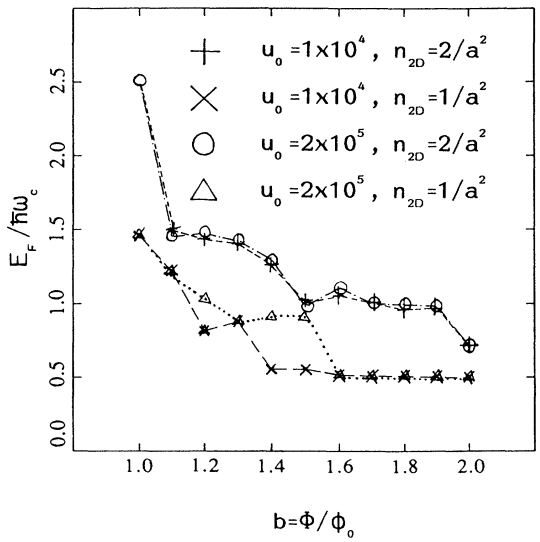

FIG. 3. The Fermi energy as a function of magnetic field for different scattering strengths and electron densities. Here, we have used $N_x=N_y=10$, $N_u=3$, and $1\le b\le 2$ in the calculations.

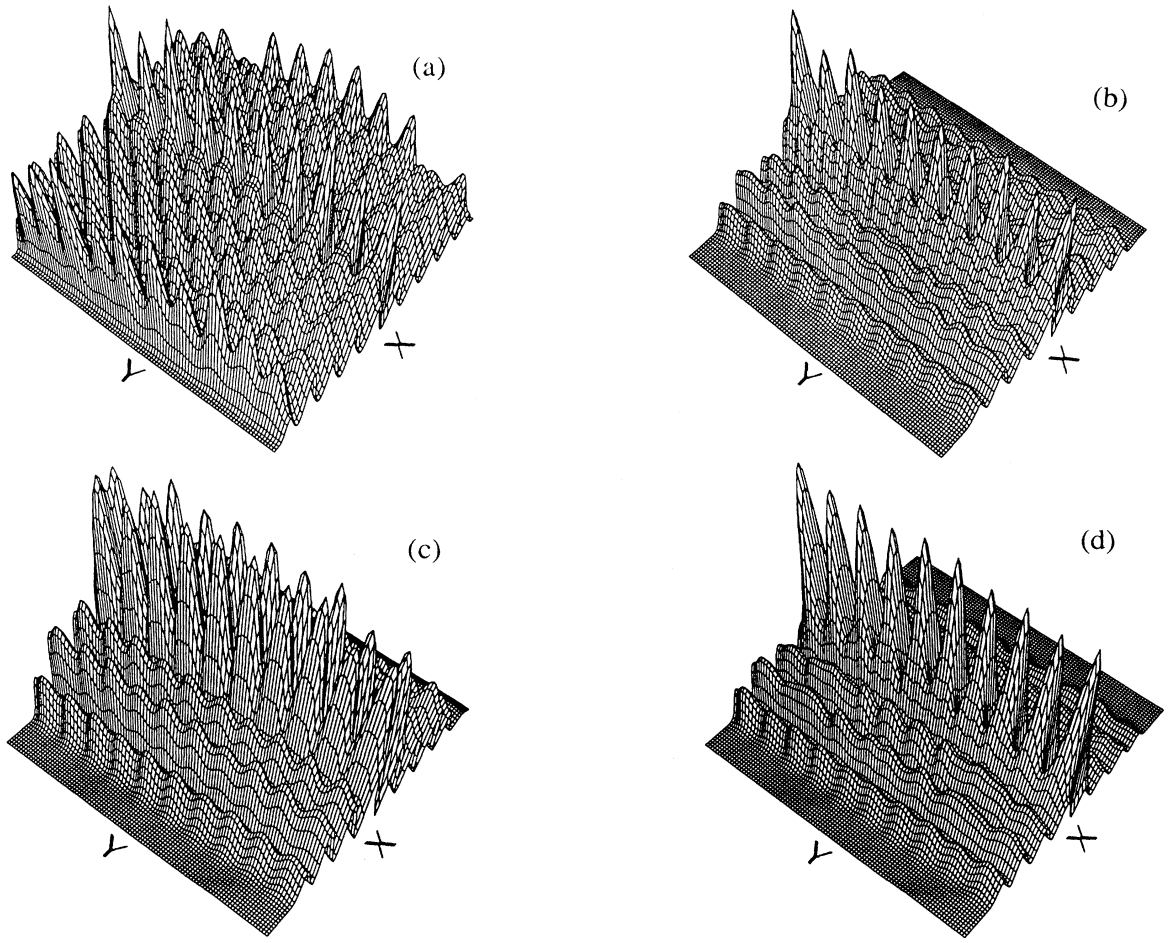

FIG. 4. The charge-density distributions for different scattering strengths, magnetic fields, and electron densities. Here, we have taken $N_x=N_y=10$, $N_u=3$, $-5\le x\le 5$, and $-5\le y\le 5$ in the calculations. (a) $b=2.0$, $u_0=1\times10^4$, $n_{2D}=1/a^2$; (b) $b=1.0$, $u_0=1\times10^4$, $n_{2D}=1/a^2$; (c) $b=1.0$, $u_0=1\times10^4$, $n_{2D}=2/a^2$; (d) $b=1.0$, $u_0=2\times10^5$, $n_{2D}=1/a^2$.

we obtain the induced Hartree potential from Poisson's equation as

$$V^{\rm ind}(q_x,q_y,\omega)=-\frac{2\pi e}{\epsilon_s q_{xy}}\delta n(q_x,q_y,\omega)\ , \tag{18}$$

where $q_{xy}=(q_x^2+q_y^2)^{1/2}$ and $\epsilon_s=4\pi\epsilon_0\epsilon_b$ with ϵ_b being the background dielectric constant. When the condition $|\sum_{q_x,q_y}e^{-i(q_x x+q_y y)}V^{\rm ext}(q_x,q_y,\omega)|/\hbar\omega\ll 1$ is satisfied, we only need to keep up to the linear term as a reasonable approximation for the time-dependent wave function, where the $\hbar\omega=12.4$ meV for $\lambda=100$ μm (far-infrared wavelength region). When this approximate wave function is used in linear-response theory,[11] we obtain the density fluctuation due to the external perturbation as

$$\delta n(x,y,t)=2\sum_{J,J'}\langle J|H_1|J'\rangle\langle J'|\delta(x-x')\delta(y-y')|J\rangle\frac{f_0(E_{J'})-f_0(E_J)}{E_{J'}-E_J-\hbar\omega}\ , \tag{19}$$

where the prefactor 2 comes from the spin degeneracy, and

$$H_1=-eV^{\rm tot}(x',y',t)=-e\sum_{q_x',q_y'}e^{i[\omega t-(q_x'x+q_y'y)]}V^{\rm tot}(q_x',q_y',\omega)\ , \tag{20}$$

with $V^{*\rm tot}(q_x',q_y',\omega)=V^{\rm tot}(-q_x',-q_y',\omega)$. The Fourier transform of Eq. (19) is given by

$$\begin{aligned}\delta n(q_x,q_y,\omega)&=\int_{-\infty}^{\infty}dx\int_{-\infty}^{\infty}dy\,e^{i(q_x x+q_y y)}\delta n(x,y,t)\\&=-2e\sum_{J,J'}\Pi_{J',J}(\omega)S_{J',J}(q_x,q_y)\sum_{q_x',q_y'}S^*_{J',J}(q_x',q_y')V^{\rm tot}(q_x',q_y',\omega)\ ,\end{aligned} \tag{21}$$

where the polarization function and the form factor are defined by

$$\Pi_{J',J}(\omega)=\frac{f_0(E_{J'})-f_0(E_J)}{E_{J'}-E_J-\hbar\omega} , \tag{22}$$

$$S_{J',J}(q_x,q_y)=\int_{-\infty}^{\infty}dx\int_{-\infty}^{\infty}dy\, e^{i(q_x x+q_y y)} \times\Psi^*_{J'}(x,y)\Psi_J(x,y) , \tag{23}$$

and $V^{\rm tot}=V^{\rm ind}+V^{\rm ext}$. $f_0(E)$ is the Fermi function and E_ν is an energy eigenvalue. Here, we neglected the exchange and correlation part $V^{\rm xc}$ which is believed to play a small role in the present problem.[5] Defining the matrix elements

$$V_{J',J}=\sum_{q_x,q_y} S^*_{J',J}(q_x,q_y)V(q_x,q_y,\omega) , \tag{24}$$

where $V_{J,J'}=V^*_{J',J}$, and making use of the self-sustaining condition $V^{\rm ext}=0$, we finally obtain the self-consistent equations

$$V_{K',K}=\sum_{q_x,q_y}\frac{4\pi e^2}{\epsilon_s q_{xy}}\sum_{J,J'}\Pi_{J',J}(\omega)S^*_{K',K}(q_x,q_y) \times S_{J',J}(q_x,q_y)V_{J',J} , \tag{25}$$

where $S_{J',J}(q_x,q_y)=S^*_{J,J'}(-q_x,-q_y)=S_{J,J'}(q_x,-q_y)$. The energies of the magnetoplasmon excitations correspond to the solutions of the secular equation

$$\mathcal{D}et\left\{\delta_{K,J}\delta_{K',J'}-\sum_{q_x,q_y}\frac{4\pi e^2}{\epsilon_s q_{xy}}\chi_{J',J}(\omega) \times S^*_{K',K}(q_x,q_y)S_{J',J}(q_x,q_y)\right\}=0 . \tag{26}$$

At $T=0$ K and in the random-phase approximation (RPA), the polarization function is given by

$$\chi_{J',J}(\omega)=\Pi_{J',J}(\omega)+\Pi_{J,J'}(\omega) =\frac{2(E^{(0)}_{J'}-E^{(0)}_J)(n_{J'}-n_J)}{\hbar^2\omega^2-(E^{(0)}_{J'}-E^{(0)}_J)^2} , \tag{27}$$

for $1\le J\le J'$, where the quantum number J is restricted to the occupied states and J' to the unoccupied states. Moreover, the occupation number can be calculated as

$$n_J=\begin{cases}0 \text{ for } J>N_{\rm tot}/2\\ 1 \text{ for } J\le N_{\rm tot}/2 .\end{cases} \tag{28}$$

The three-level model can be solved analytically. When more than three energy levels are included, we must solve Eq. (26) numerically. In general, the spectrum is obtained from the following eigenvalue equation:

$$\mathcal{D}et[\,\mathbf{A}-\hbar^2\omega^2\mathbf{I}]=0 , \tag{29}$$

where $\mathbf{I}$ is the unit matrix, and the matrix $\mathbf{A}$ is defined by

$$\mathbf{A}_{K,J}=\Delta^2_{J,0}\delta_{K,J}+2\Delta_{J,0}\left[\sum_{q_x,q_y}\frac{4\pi e^2}{\epsilon_s q_{xy}}S^*_{K,0}(q_x,q_y) \times S_{J,0}(q_x,q_y)\right] . \tag{30}$$

Here, the off-diagonal matrix elements in Eq. (30) correspond to the coupling between transitions to different excited states.

In our numerical calculations, we have taken $n_{2D}=1/a^2$ so that $N_{\rm tot}=N_xN_y$. Furthermore, the Landau-level filling factor is $\nu_L=2\pi L_H^2 n_{2D}=1/b$. For each level, we have $2M_u=bN_xN_y$ allowed states. If $b\ge 1$ we have $2M_u\ge N_{\rm tot}/2$ or $\nu_L\le 1$. In our calculations, we take $N_x=N_y=10$, $N_{\rm tot}=100$, $N_u=3$, $n_{2D}=1/a^2$, $m^*=0.067m_e$ (m_e is the free-electron mass), $a=31.6$ nm, and $\epsilon_b=12.5$. Furthermore, we have chosen $J=N_{\rm tot}/2$ for the highest occupied state and $J=N_{\rm tot}$, $2M_u+1$, $3M_u$ for the unoccupied states, as shown in Figs. 5(a) and 5(b). From Figs. 5(a) and 5(b) we see that the transition with constant $\Delta J=N_{\rm tot}/2$ is associated with the intra-Landau-level transition or *edge mode* at strong magnetic field, while the transitions to the levels with $J=2M_u+1$, $3M_u$ are related to inter-Landau-level transitions or *cyclotron modes* at strong magnetic field. For cyclotron modes, ΔJ depends on magnetic field; this is due to the increase in Landau-level degeneracy with magnetic field. At low magnetic fields, the edge mode with $J=N_{\rm tot}$ has an energy which is higher than that of the excited state with $J=2M_u+1$. Here, both the Fermi energy and the energy of the excited state with $J=2M_u+1$ follow the third Landau level, while the edge mode and the excited state with $J=3M_u$ follow the fourth Landau level. Due to mixing of the umklapp scatterings, some states in the first two Landau levels are scattered into higher energy levels. This leads to the original second Landau-level state with $J=3M_u$ developing into a third Landau-level state at strong magnetic field. All three excited states are separated at $b=1$, which is independent of u_0. There is a level crossing between edge and excited states at $b=1.2$ under strong

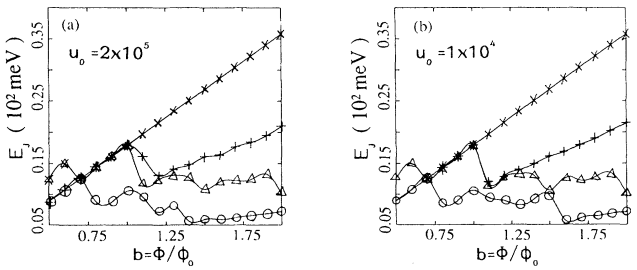

FIG. 5. Eigenenergy levels E_J for the excited states and Fermi energy as a function of the magnetic field with different scattering strengths. Here, we have chosen $N_x=N_y=10$, $N_u=3$, $m^*=0.067m_e$, $a=31.6$ nm, $n_{2D}=1/a^2$, and $0.5\le b\le 2.0$ in the calculations. The notations, i.e., (○), (△), (+), and (×), correspond to $J=N_{\rm tot}/2$, $N_{\rm tot}$, $2M_u+1$, and $3M_u$, respectively. (a) $u_0=2\times10^5$; (b) $u_0=1\times10^4$.

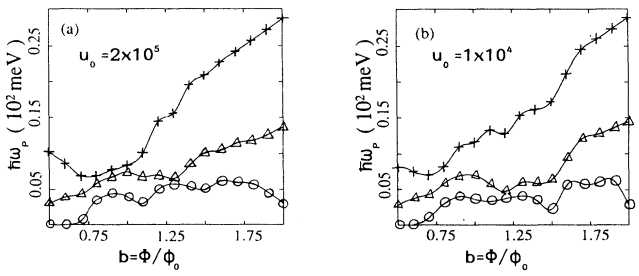

FIG. 6. Energy of magnetoplasmon excitations for antidots as a function of magnetic field for different scattering strengths. Here, we have used $N_x=N_y=10$, $N_u=3$, $a=31.6$ nm, $n_{2D}=1/a^2$, $m^*=0.067m_e$, $\epsilon_b=12.5$, and $0.5\le b\le 2.0$ in the calculations. We have chosen the transitions from the topmost occupied state $J=N_{\rm tot}/2$ to the unoccupied states $J=4N_{\rm tot}/5$ (○), $2M_u+1$ (△), $3M_u$ (+). (a) $u_0=2\times10^5$; (b) $u_0=1\times10^4$.

scattering. The second and third Landau-level states are largely unaffected except at low magnetic fields, while the edge and the highest occupied states are strongly modulated by the scattering.

Figures 6(a) and 6(b) show the magnetoplasmon energies as a function of magnetic field for different scattering strengths. For strong scattering, we can see two anticrossings at $b=0.8$ and 1.3, respectively. The higher one is related to the coupling between the edge mode and the $2\omega_c$ cyclotron mode, while the lower one is due to the coupling between the ω_c cyclotron mode and the edge mode. There is a threshold field for the lowest branch of magnetoplasmon excitation, below which the gap becomes negligible. In weak magnetic fields, we clearly see the negative dispersion and oscillation of the magnetoplasmon energies for the edge modes before going into the upper anticrossing region. The change with scattering strength becomes obvious at strong magnetic field. The Coulomb interaction lifts the degeneracy in the single-particle energy eigenvalues due to the differences in screening at weak magnetic fields. Our calculations show that the effect due to the Coulomb interaction is small when the magnetic field is strong.

The negative B dispersion of the edge modes is mainly due to the lifting of the degeneracy by the Coulomb interaction between the excited state with $J=3M_u$ and the edge mode with $J=N_{\rm tot}$. It is also a result of an increase in the Landau-level degeneracy with magnetic field which leads to the usual negative dispersion for the edge state. The oscillating dispersion of the edge modes is attributed to the oscillations in the Fermi energy and the energy of the edge states, i.e., the resonant coupling between the umklapp scatterings [see Figs. 5(a) and 5(b)]. The anticrossing is a direct result of the Coulomb interaction between electrons. This anticrossing is partly smeared out when the scattering is weak. The occurrence of the $2\omega_c$ cyclotron mode is the fact that some degenerate states in the first two Landau levels have been raised to higher energy levels, involving the original second Landau-level excited state with $J=3M_u$ into a third Landau-level state. Also, the mixing of the Landau wave functions ensures the nonvanishing intensity for this optical transition.

IV. CONCLUSIONS AND DISCUSSION

In conclusion, we have calculated exactly the single-particle energy eigenvalues and eigenfunctions for a square array of quantum antidots in a perpendicular uniform magnetic field. Quantum mechanically, we have found significant effects due to scattering. The strong mixing of the Landau bands, due to the resonant coupling between umklapp scatterings, is clearly shown. The peaks in the Fermi energy imply that some states have been raised to high energy levels. Our calculations display many of the features for magnetoplasmon excitations which have been reported in a recent experiment on antidots.[9]

Due to the strong spatial modulation arising from the potential scatterers, we cannot use a perturbation approach to obtain the single-particle energies, thereby making numerical calculations essential. Comparing our numerical results with experimental measurements by Kern *et al.*,[9] we find that the basic features in the measurement have been reproduced by our present simple model, including the oscillations, negative dispersion, and anticrossing. We emphasize that this agreement is only qualitative and not quantitative. The disagreement between our model calculations and the experimental data is due to setting the radius of the core equal to zero. However, the basic features predicted here should not be changed qualitatively if the radius of the core is taken to be much smaller than the lattice constant. For a finite core radius, we must modify the matrix elements in Eq. (12) when calculating the eigenstates. This would, of course, change the polarization function in Eq. (27) as well as the form factor in Eq. (23).

In order to present a clear analysis of the physics involved, we only include four energy levels in our numerical calculations of the magnetoplasmon excitation energies. In principle, all the occupied states and the low-energy unoccupied states, excluding those with much higher energy levels, should be included. Unfortunately, this makes the dimensionality of the matrix in Eq. (30) too large for our computational facilities. However, we believe that the qualitative feature displayed in Figs. 6(a) and 6(b) will not change for larger determinants.

ACKNOWLEDGMENTS

This work was supported in part by a grant from the Natural Sciences and Engineering Research Council of Canada and a program of the City University of New York.

[1]C. Sikorski and U. Merkt, Phys. Rev. Lett. **62**, 2164 (1989).
[2]T. Demel, D. Heitmann, P. Grambow, and K. Ploog, Phys. Rev. Lett. **64**, 788 (1990).
[3]A. Lorke, J. P. Kotthaus, and K. Ploog, Phys. Rev. Lett. **64**, 2559 (1990).
[4]A. Kumar, S. E. Laux, and F. Stern, Phys. Rev. B **42**, 5166 (1990).
[5]D. Huang and G. Gumbs, Phys. Rev. B **43**, 12 039 (1991).
[6]M. Wagner, U. Merkt, and A. V. Chaplik, Phys. Rev. B **45**, 1951 (1992).
[7]R. R. Gerhardts, Phys. Rev. B **45**, 3449 (1992).
[8]N. F. Johnson and M. C. Payne, Phys. Rev. B **45**, 3819 (1992).
[9]K. Kern, D. Heitmann, P. Grambow, Y. H. Zhang, and K. Ploog, Phys. Rev. Lett. **66**, 1618 (1991).
[10]D. Weiss, M. L. Roukes, A. Menschig, P. Grambow, K. v. Klitzing, and G. Weimann, Phys. Rev. Lett. **66**, 2790 (1991).
[11]A. L. Fetter and J. D. Walecka, *Quantum Theory of Many-Particle Systems* (McGraw-Hill, New York, 1971), p. 172.